frontiers in Earth Science

ORIGINAL RESEARCH
published: 02 December 2021
doi: 10.3389/feart.2021.792280

Characterizing Concealed Fault Systems by Integrating Field Data Mapping and Laboratory Experiments: A Case Study of the Huawa Area in East China

Huiting Hu[1,2], Shuang Hu[2], Rui Zhang[3], Xiaofei Fu[4,5], Chongyu Ren[1]*, Qidong Liu[6], Wenquan Yu[7] and Yuchen Yang[7]*

[1]School of Earth Sciences, Northeast Petroleum University, Daqing, China, [2]CNPC Fault Controlling Reservoir Laboratory, Northeast Petroleum University, Daqing, China, [3]School of Geosciences, University of Louisiana at Lafayette, Lafayette, LA, United States, [4]Key Laboratory of Continental Shale Hydrocarbon Accumulation and Efficient Development Ministry of Education, Northeast Petroleum University, Daqing, China, [5]Heilongjiang Institute of Technology, Haerbin, China, [6]Institute of Geological Sciences, Jiangsu Oilfield Branch, Yangzhou, China, [7]Geology and Geophysics Program, Missouri University of Science and Technology, Rolla, MO, United States

OPEN ACCESS

Edited by:
Kouqi Liu,
Central Michigan University, United States

Reviewed by:
Min Wang,
China University of Petroleum (Huadong), China
Ming Ma,
Chang'an University, China

***Correspondence:**
Shuang Hu
hu-shuang@foxmail.com
Chongyu Ren
renchongyu1234567@163.com

Specialty section:
This article was submitted to Economic Geology, a section of the journal Frontiers in Earth Science

Received: *11 October 2021*
Accepted: *09 November 2021*
Published: *02 December 2021*

Citation:
Hu H, Hu S, Zhang R, Fu X, Ren C, Liu Q, Yu W and Yang Y (2021) Characterizing Concealed Fault Systems by Integrating Field Data Mapping and Laboratory Experiments: A Case Study of the Huawa Area in East China. Front. Earth Sci. 9:792280. doi: 10.3389/feart.2021.792280

Concealed faults can be important for understanding the regional structural geology and the subsurface fluid distribution. However, such faults are usually difficult to identify and characterize because of their small size and complex mechanism. To address this issue, we present an integrated approach of three-dimensional seismic data mapping and physical modeling experiments to examine the geometrical and kinematic characteristics of concealed faults and their relationship with the main faults in the Huawa area, east China. Three series of experiments were designed to characterize the differences in the scale of concealed faults and main faults, which also allowed us to examine how the concealed faults grow with the main faults in the area. Through this integrated study, we have demonstrated that: 1) NE-SW-striking concealed faults are below the resolution of the available seismic datasets and not easily recognized in seismic sections and that most of them grew later than the E-W-striking main faults, with some of them having grown at the same time; 2) pre-existing faults, rather than asymmetry of the basin structure, affect the faults that develop during subsequent episodes of extension; 3) E-W-striking pre-existing faults under a NW-SE stress direction of extension are most likely the formation mechanism of concealed faults. This study is of reference value in the interpretation of concealed faults in other regions.

Keywords: concealed faults, formation mechanism, three-dimensional seismic data, sandbox physical simulation model, gaoyou Sag, transfer zone

INTRODUCTION

Concealed faults usually grow with main faults but appear smaller in size, which makes it difficult to recognize and characterize them. In the refined stage of oil and gas exploration, concealed faults can play an important role in understanding the regional structural geology and characterizing the subsurface fluid distribution. There are two main aspects: 1) concealed faults are associated with

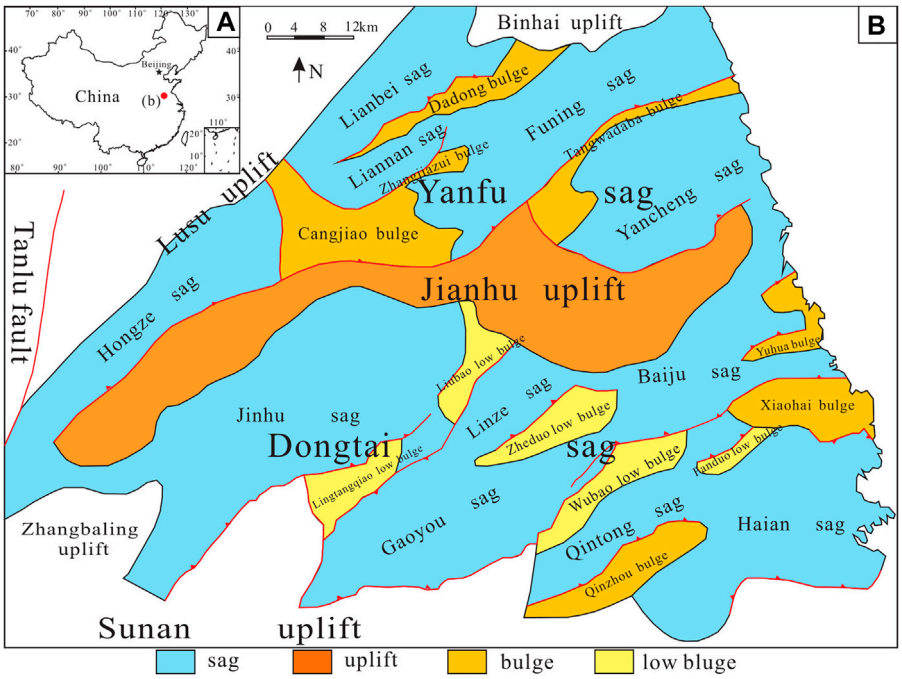

FIGURE 1 | Tectonic units of the North JiangSu Basin. **(A)** Location of North JiangSu Basin in China; **(B)** Huawa area is located in the east of Gaoyou sag , the south of North JiangSu Basin.

large-scale faults, and they often form fault block traps with large-scale faults, which cannot be identified effectively, resulting in the omission of favorable exploration targets (Li, 2014). 2) Concealed faults that act as compartments within the reservoir failed to correctly identify sectionality, and closure led to the wrong development plan, resulting in ineffective water injection in most wells (Rotevatn and Fossen, 2011). Therefore, it is necessary to identify concealed faults and analyze their petrophysical properties in oilfield exploration (Gong et al., 2021). Three-dimensional seismic data mapping is one of the most effective ways to locate concealed faults but lacks information about their history and mechanism.

In this paper, we present a set of laboratory experiments in combination with field mapping results to investigate the history, distribution, and mechanism of concealed faults associated with main faults in the Huawa area, east China. The study area is located in the Gaoyou Sag, a sub-basin in Jiangsu province, China (Dong et al., 2013; Li et al., 2013; Chen et al., 2015; Qiu et al., 2016), which is an intensely faulted area with very complex fault systems. The Gaoyou Sag is bounded on the west by the Lingtangqiao Low Uplift and the Liubao Low Uplift, on the south by the Sunan Uplift, on the east by the Wubao Low Uplift, and the Zheduo Low Uplift extends into Gaoyou Sag on the northeast (**Figure 1**). The energy industry has explored this area for years, which has provided us with plentiful geological and geophysical information. From well-log information (hua3, hua4, hua11, and hua12, shown in **Figure 2**), it has been reported that the NE-SW-striking concealed faults existing in the Huawa area control the subsurface fluid movements. However, the formation mechanism of the concealed faults remains unclear, which makes it difficult to understand them. The purpose of this paper is to demonstrate the geometric and kinematic characteristics of the concealed faults in relation to the main faults in the Huawa area and to analyze the formation mechanism of concealed faults by combining the above characteristics with the results from three series of physical laboratory experiments.

GEOLOGIC BACKGROUND

The North Jiangsu Basin is a Cenozoic rift basin with a Mesozoic and Paleozoic basement (Yang and Chen, 1989). The North Jiangsu basin was formed during the late Cretaceous Yizheng event and then experienced two major tectonic events, Wubao and Sanduo. Each tectonic event had a great influence on the sedimentary pattern and tectonic pattern of the basin (**Figure 3**). According to the characteristics of tectonic movement and the sedimentary filling sequence, the basin evolution can be divided into three stages (Mao, 2000; Wang et al., 2001; Hu, 2010).

1) Wubao stage (K_2t–E_1f_4). During this period, the overall topography of the basin was high in the west and low in the east, with a fault in the south and a lift in the north. At the early stage of fault depression, that is, the K_2t_1 deposition stage, first-level faults formed in the depression and began to be active, and these controlled both the formation thickness and distribution of sedimentary facies zones. Subsequently, lacustrine transgression began, and K_2t_2 dark mudstone and marl were deposited, but the range of lacustrine transgression was limited to the central and eastern sag. The Paleocene basin

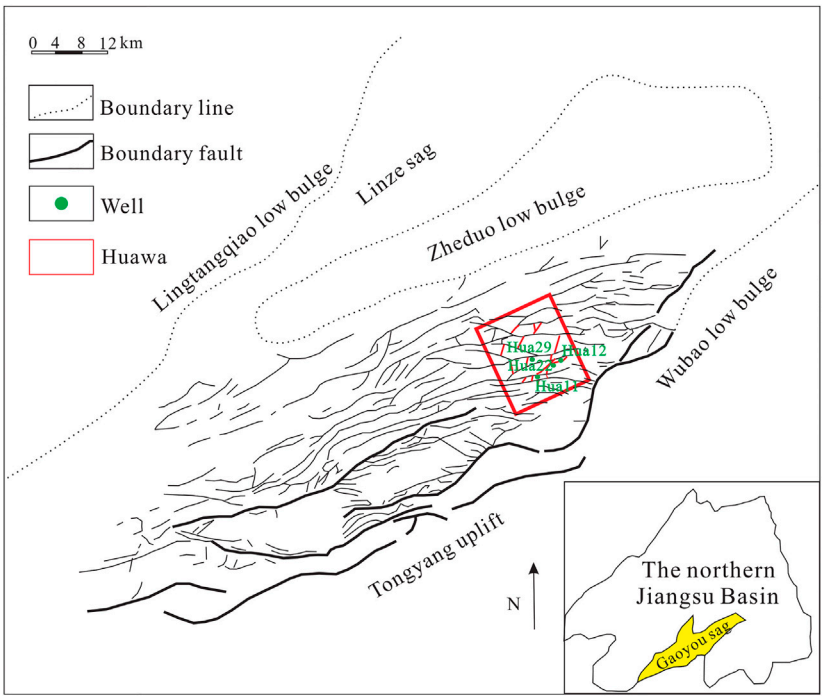

FIGURE 2 | Fault system distribution in the Gaoyou sag.

underwent two more lacustrine transgressions with an obviously larger scope than the transgression of the early stage, which affected the whole basin and even the southern Jiangsu area in the south of the basin.

Longitudinally, the strata during this period include three complete coarse-fine-coarse sedimentary cycles: K_2t_1–K_2t_2, E_1f_1, and E_1f_2–E_1f_3. In the Tertiary period, E_1f_4 experienced one of the largest lacustrine transgressions, which was basically composed of a set of dark mudstone. Only a small amount of deltaic sandstone existed on the west side of the Jinhu sag in the west part of the basin, and the top suffered extensive denudation under the influence of the Wubao event. In the middle of each cycle affected by flooding, the main Cenozoic basin in the north Jiangsu source sequence is formed gradually. Different depositional environments formed depending on the degree of flooding, and good source rocks are formed in the water inflow stage, for example, at the bottom of K2t2, the top of E1f2, and the upper-middle of E1f4; the source rocks of each cycle are formed with good oil- and hydrocarbon-generating conditions. Three complete cycles resulted in lower sedimentary environments for river deltas, alluvial plains, alluvial fans, and fan deltas, which represent four types of good reservoirs.

2) Sanduo stage (E_2d_1–E_2s_2). The Wubao event at the end of the Paleocene divided the wide lake basin, which was uniformly deposited during the early transgression, into several sedimentary units with the sag as a unit. In the Sanduo period, multiple sedimentary systems were developed in each depression, a series of nearshore underwater fan and fan deltas were developed in steep slope zones, and large delta sedimentary systems or fluvial sedimentary systems were developed in gentle slope zones. The large faults at the boundary and the secondary faults in the depression obviously controlled the deposition. Tectonic activity is characterized by strong fault depression and a significant difference in the rise and fall of the fault upper and footer, and the fault distance of most faults exceeds 1,000 m. On the whole, it is strong in the west and weak in the east. For example, the thickness of the E_2s and E_2d deposition in the Hongze, Jinhu, and Gaoyou sags in the west is larger than the thickness in the Haian, Baiju, and Yancheng depressions in the east. In particular, the Gaoyou sag has the largest subsidence range, and the maximum thickness of the deposited strata exceeds 2,500 m.
3) Yancheng stage (Ny_1–Ny_2). The basin or depression was basically flattened after filling, and deposition occurred in the Eocene and tectonic transformation in the Oligocene. Next, there was an overall decline leading to the depression development stage. Thick alluvial plain facies were filled and deposited during this period. The magmatic activity during this period was dominated by alkaline basalts of continental type.

There were three important geological events in the tectonic history of the basin. The Yizheng event (83 Ma) laid the

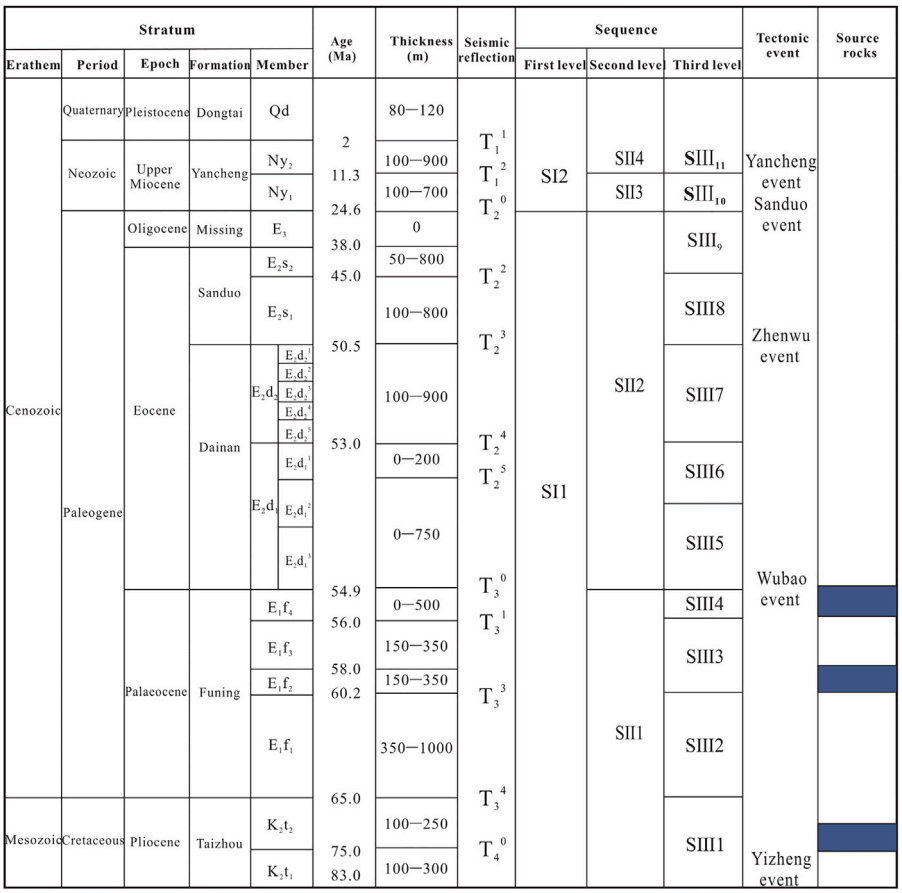

FIGURE 3 | Comprehensive stratigraphic column showing the major tectonic events and sedimentary sequences in the Subei Basin. Yizheng and Wubao movements controlled the formation evolution of the Gaoyou sag.

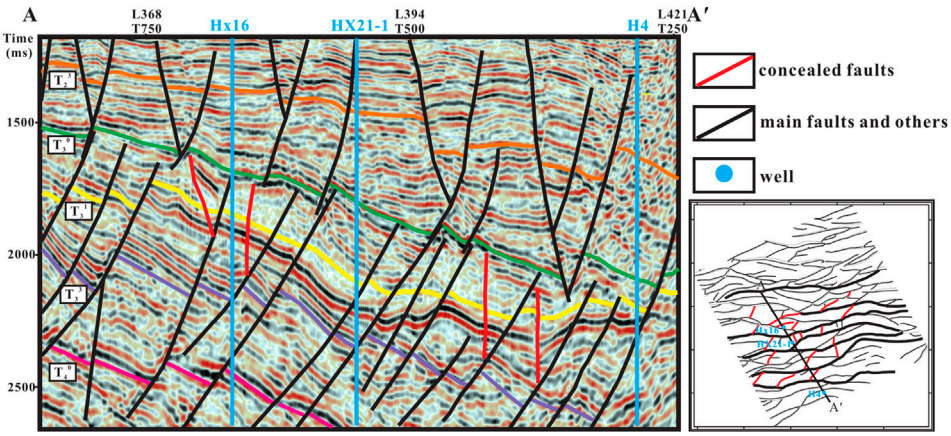

FIGURE 4 | (A) seismic cross-section with some well-logs, multiple horizons, including T_3^1 and others, main faults, and concealed faults.

foundation of the basin. The Wubao incident (54.9 Ma) caused the whole fault depression basin to disintegrate and finally completed the development of fault depression. The Sanduo event (38 Ma) raised the whole basin, which experienced long-term intense denudation, and then, the basin returned to a new round of depression and gradually disappeared.

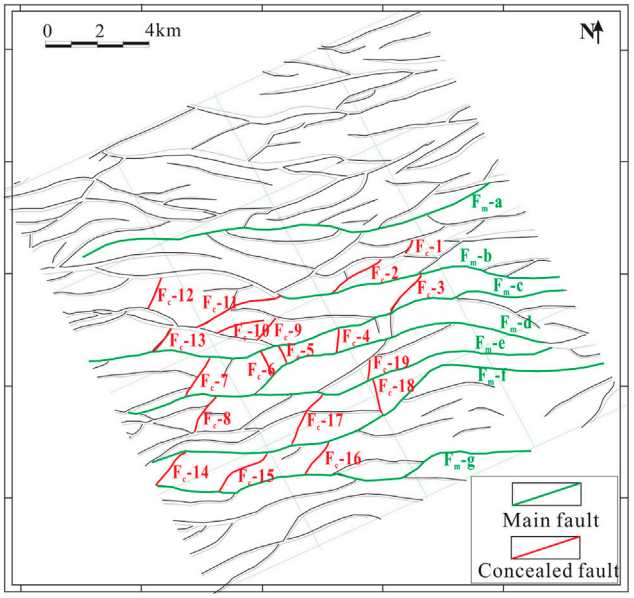

FIGURE 5 | The T_3^1 structural map of Huawa area including main faults and concealed faults.

Fault activity caused by geological events is the main manifestation of the Meso-Cenozoic tectonic movement in the North Jiangsu basin. They control the deposition, loss, and denudation of sediments in the depression and the distribution of the sequence and system domain.

FAULT NETWORK IN THE HUAWA AREA

3D Seismic Data Mapping

In seismic sections, a conventional method is used to interpret the main faults, which are characterized by obvious dislocation in seismic events. The concealed faults are not easily identified in the Line or Crossline section, so an arbitrary line almost perpendicular to the concealed faults is used to define the seismic section (**Figure 4**), which maximizes the shown throw of the concealed fault, so that the fault response becomes clearer.

Geometric Distribution of Concealed Faults

The top T_3^1-structure map best illustrates the geometry of the Huawa area fault network (**Figure 5**). Deformation is dominated by the E-W-striking main faults, along with a series of short, NE-SW-striking concealed faults among them. We have mapped out 19 concealed faults and seven main faults in the Huawa area, highlighted by the red color and the green color, respectively, in **Figure 5**. The extension length, maximum fault throw, and fault strike are presented in **Table 1**, and comparative statistics are shown in **Figure 6**. The NE-SW-striking concealed faults extend 1–3 km, with a fault throw between 10 and 80 m and with most fault throws less than 10 m at the T_3^1 structural surface. In contrast to the concealed faults, E-W-striking main faults extend 3–5 km, and the fault throw is generally between 50 and 300 m. It is obvious that the E-W-striking main faults are larger than the NE-SW-striking concealed faults.

TABLE 1 | Summary of concealed fault elements.

Number	Length (m)	Extending direction	Fault throw (m)
1	813	230	50
2	2070	219	72
3	1906	228	17
4	922	261	14
5	879	292	14
6	815	295	14
7	1737	237	24
8	1,529	238	11
9	1,068	229	38
10	1,534	199	10
11	1,491	190	10
12	1,403	246	10
13	1,143	236	32
14	1,451	231	23
15	2,119	221	74
16	1,424	235	70
17	2022	241	80
18	1,529	283	19
19	963	266	36

In the case of large fault throws, the concealed faults can be identified from the seismic profiles, which are perpendicular to the strike direction of concealed faults. However, in most cases, the fault throw of concealed faults is less than 10 m. Even if the seismic profiles, which are perpendicular to the concealed faults, are selected, only the lined-up distortions can be seen, which results in great uncertainty for their identification. Therefore, it is necessary to study the formation period and formation mechanism of concealed faults, in order to provide a theoretical basis for the identification of concealed faults.

Kinematic Characteristics of Faults

The growth index is one of the important parameters that determine the time and rate of stretching and extrusion of fault activity (Thorsen, 1963; Zhao, 1989). The growth index reflects the growth rate of the fault, such as the intensity. The larger the ratio of the growth index, the greater the intensity of the fault activity (Liu et al., 2021). Based on the ratio of the growth index, the kinematic characteristics of the fault can generally be described as follows: ① When the fault growth index is equal to 1, the thickness of the two plates is equal. As such, faulting in this interval is interpreted to be post sedimentary, and the period is one of fault inactivity and burial; ② When the fault growth index is greater than 1, the thickness of the hanging-wall is greater than that of the footwall, and syndeposit normal faulting occurs. The larger the growth index value, the larger the normal breaking rate. During the period of the most intense fault activity, that is, when the strata of the descending disk grow the most, the growth index shows the maximum value, which can reach between 5 and 10; ③ When the fault growth index is less than 1, the thickness of the hanging-wall is less than the thickness of the footwall, indicating that the fault is active, the fault is a reverse fault, and that syndeposit reverse faulting (extrusion) occurs. The smaller the

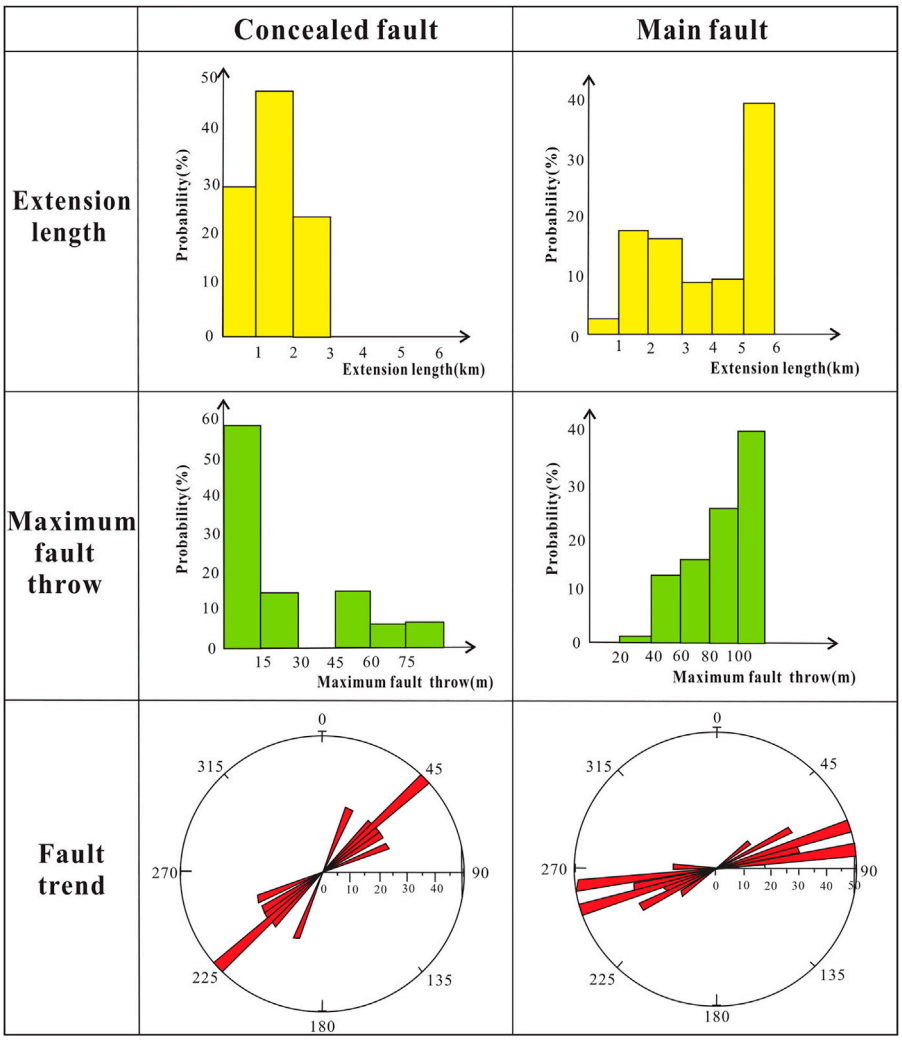

FIGURE 6 | Summary of fault extension length, maximum fault distance, and fault strike of concealed and main faults in the Huawa area.

growth index value, the higher the reverse fault rate. The larger the growth index of the normal fault or the smaller the growth index of the reverse fault, the stronger the fault activity.

In addition to the growth index, the variation in the fault throw with depth is also used to characterize the kinematic characteristics of faults (Ryan et al., 2017; Sun and Lu, 2017; Rashidi, 2021). Fault growth is a dynamic process in the historical period. The characteristics of fault activity are different under different tectonic and sedimentary backgrounds (Liu, 2017). By measuring the fault inclinations at different depths on the geological profile, we can determine the active period of the fault. In general, the fault throw is largest at the location where the fault is initially formed, which is called the 'nucleus point' (Wang, 2018). The process of fault formation and evolution can be divided into four types: ① Isolated fault type, where the 'fault throw-depth' relationship curve looks like 'C,' the fault throw is largest at the center of the vertical direction and smallest at the end, and there is only one "nucleus point" (**Figure 7A**), indicating that the fault is only active for one period; ② Continuous growth type, where the "fault throw-depth" relationship curve shows linear growth, and the fault distance and buried depth curve show a linear increase, indicating that fault activity and deposition occur simultaneously (**Figure 7B**); ③ Fault reaction type, where the lower part of the "fault throw-depth" relationship curve shows a continuous linear growth, with an obvious upward inflection point, and where the upper part has obvious inflection points and the fault throw gradient decreases rapidly. Compared with the continuous growth type, it has an interval and burial period and then activates and grows upward (**Figure 7C**); ④ Dip connection type, where the "fault throw-depth" relationship curve looks like 'M'; it has two distance maxima and one minimum in the middle (**Figure 7D**), indicating that the upper and lower faults are active until the final connection.

In **Figure 8**; **Figure 9**, we show two kinds of main faults in the Huawa area according to the different degrees and styles of kinematic characteristics: 1) The growth indexes of the K_2t_2–E_1f_1 and E_1f_2–E_1f_3 strata are above 1. In addition, the T-z profiles, which reflect the relationship between fault throw

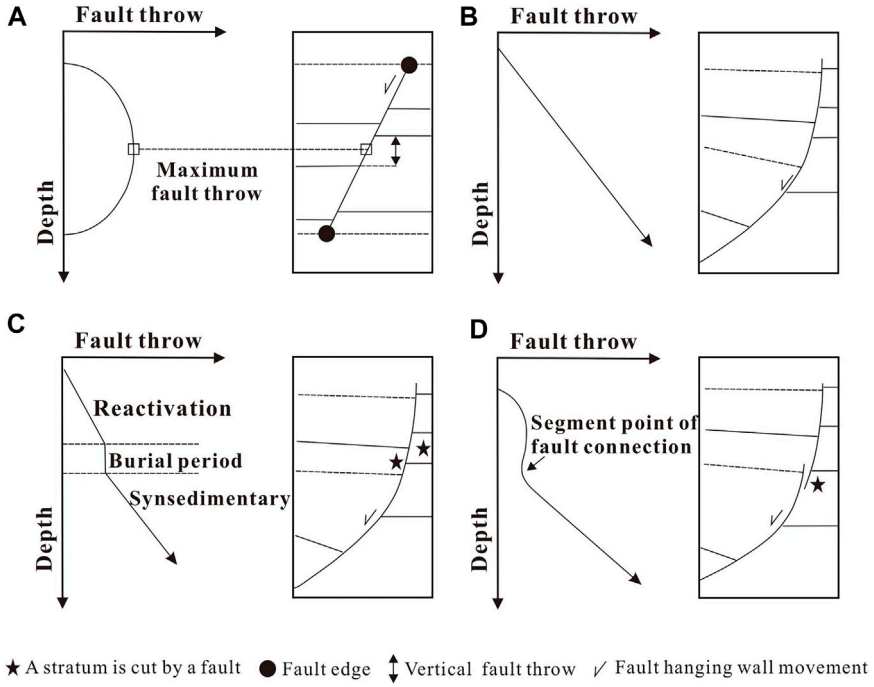

FIGURE 7 | The model diagram of the fault throw-depth curve. **(A)** Isolated fault type; **(B)** continuous growth type; **(C)** fault reactivation type; and **(D)** dip connection type. Modified from Wang *et al.* (2020).

and depth, indicate that the throw grows with depth in these two intervals of growth strata. The research results suggest that during the K_2t_2–E_1f_3 sedimentary period, this kind of main fault was an active category (**Figure 8**); 2) The growth index of the K_2t_2–E_1f_1 stratum is close to 1, while that of the E_1f_2–E_1f_3 stratum exceeds 1. In addition, according to the T-z profiles, main faults of this kind slightly approach the upper tip or generally follow a symmetric line. On the T-z profiles, the point of maximum throw, which is often interpreted to indicate where fault nucleation occurs, generally locates at the T_3^3 of the stratigraphic level since throw decreases to the upper and lower tips. Therefore, we conclude that main faults of this kind were active only during the E_1f_2–E_1f_3 sedimentary period, with fault nucleation occurring in the E_1f_1 succession (**Figure 9**). On the whole, most of these faults belong to the isolated fault type and continuous growth type, but the active period and intensity of the faults are different. The active period of main faults is earlier and longer than that of concealed faults, and the activity intensity is higher. The concealed faults also indicate two different degrees and manners of kinematic characteristics: 1) One type of concealed fault is the same as the second style mentioned previously, with fault nucleation occurring in the E_1f_1 succession, and this kind of fault was active only during the E_1f_2–E_1f_3 sedimentary period; 2) The other kind of concealed fault is planar, with upper tips commonly locating in the E_1f_4 succession and lower tips in E_1f_1 sediments. The growth index of the E_1f_2–E_1f_3 stratum equals to 1, and the throw of these concealed faults varies slightly with depth. Consequently, we conclude that faults in this succession are post sedimentary and were active after the E_1f_3 sedimentary period. Therefore, it can be deemed that: 1) Concealed faults developed simultaneously or lagged behind main faults; 2) concealed faults and main faults may have metabolic connections and/or mechanical interactions; and 3) there are multiphase rifts in the Wubao Rift Phase period.

FORMATION MECHANISM OF CONCEALED FAULTS

Hypothesis of Fault Genesis

Faults usually develop within a single-phase extension, commonly strike to the extending direction in a sub-perpendicular mode, and follow a collinear or en echelon construction (Gawthorpe and Leeder, 2000). In the single-rift phase, faults with strikes oblique to the chief rift tendency may develop due to the breaking relay zones or fluctuation in the local stress area surrounding pre-existing or normal faults with broad synchronous characteristics (Maerten et al., 1999; Deng et al., 2017; Uchida et al., 2021).

However, faults without collinear distribution will not broadly develop in the fault network. Their scopes of interaction and general impact are usually low during the development of the fault network. To the contrary, in multi-phase rifts, and especially when each rift phase extends in a different direction, faults developed during the first rift phase influence the property of stress in the upper crust in the second rift phase (Bellahsen and Daniel, 2005; Whipp et al., 2013). Under this circumstance, the rift phase that follows will show reactivation in faults existing

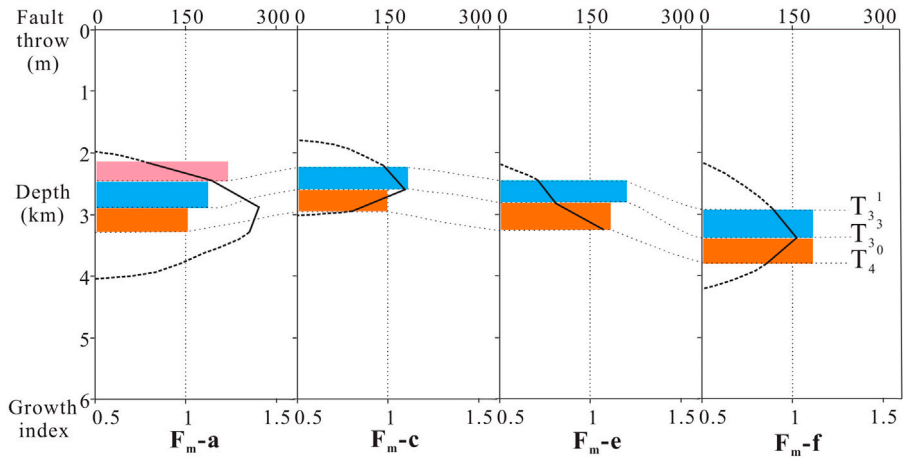

FIGURE 8 | Growth index and 'fault throw-depth' relationship curve (T-z profile) of main faults. The blue, orange, and pink rectangles indicate the growth index, corresponding to the lower coordinate axis. The black polyline indicates the 'fault throw-depth' relationship curve, corresponding to the upper coordinate axis.

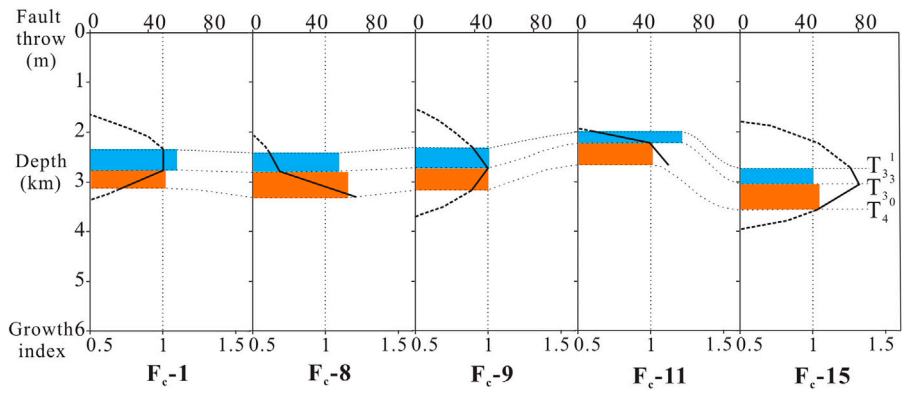

FIGURE 9 | Growth index and 'fault throw-depth' relationship curve (T-z profile) of long-term active concealed faults. The blue and orange rectangles indicate the growth index, corresponding to the lower coordinate axis. The black polyline indicates the 'fault throw-depth' relationship curve, corresponding to the upper coordinate axis.

beforehand from the first rift stage and/or nucleation in second stage faults developed recently in crust previously unruptured, which usually develop in a sub-perpendicular manner to the new extending direction (Bailey et al., 2007; Henza et al., 2010; Kulikowski et al., 2016; Gong et al., 2019). Accordingly, the following three assumptions were made in conducting our mechanism studies: ① Asymmetry in the basin structure with no pre-existing faults. The Huawa area is part of the Gaoyou sag, which has boundaries with different strikes, and the geological structure of the Gaoyou sag is narrower in the west and wider in the east. If there is no pre-existing fault, can a fault network with co-existing E-W-striking main faults and NE-SW-striking concealed faults be developed during a single rift phase? This is the first assumption. ② Asymmetry in the basin structure with NE-SW-striking pre-existing faults in the Huawa area. The second assumption infers that there were multiphase rifts. The K_2t_2–E_1f_3 sedimentary period is the second rift phase with NE-SW-striking pre-existing faults in the Huawa area. Then, E-W-striking faults formed between NE-SW-striking pre-existing faults. Under the action of tectonic stress, the E-W-striking faults steadily developed into main faults and eventually formed the structural pattern in the Huawa area. ③ Asymmetry in the basin structure with E-W-striking pre-existing faults in the Huawa area. The K_2t_2–E_1f_3 sedimentary period also seems to be the second rift phase but with E-W-striking pre-existing faults in the Huawa area. The E-W-striking faults are the pre-existing faults, and the NE-SW-striking faults are the secondary ones.

Experimental Approaches

To investigate the formation mechanism of the concealed faults in combination with the field mapping results, we used a sandbox

FIGURE 10 | Physical simulation experimental instrumentation.

physical simulation experiment in the laboratory, as shown in **Figure 10**. The experiments are expected to answer the following two questions:

1) Is it the asymmetry of the basin structure or the pre-existing fault that affects the faults that develop during subsequent episodes of extension?
2) How did the concealed faults grow in the Huawa area, under different striking pre-existing faults?

Experimental Materials

Dry quartz sand and wet clay are the most common physical modeling materials for laboratory experiments. Furthermore, the dry, loose quartz sand is an ideal material for modeling the brittle rock strata in the upper crust since its deformation meets the Mohr-Coulomb fracture criterion and is very similar to the brittle deformation behavior of the sedimentary rocks in the shallow crust (<10–15 km) (Byerlee and Wyss, 1978; Krantz, 1991; Schellart, 2000). In this study, we use dry quartz sand as the modeling material, with a particle size of 0.15–0.2 mm, an internal friction angle of 34, and an internal friction coefficient of 0.67. For most sedimentary rocks, the friction coefficient ranges between 0.55 and 0.85 (Byerlee and Wyss, 1978; Handin, 1966). Thus, the dry quartz sand used in our models (with a friction coefficient of 0.55) is a suitable modeling material.

Model Design

In the experiment, a uniformly deformed and extendable rubber sheet was used to simulate the basement weak zone (Zhao et al., 2005; Ning and Tang, 2009). Two rigid sheets (one fixed and one mobile) were designed for orthogonal extension in the model. When the stretching direction changes, the rubber sheet is rotated according to the stretching direction. The base of the apparatus consisted of a 50-cm-wide rubber sheet attached to two rigid sheets, and another rubber sheet was used to cut out the basin shape and overlaid the first layer of the rubber sheet. A layer of dry sand covered the rubber sheet layer, including the single rubber sheet, and the double rubber sheet. The layer above the double rubber sheet was 2.2-cm thick, and the layer above the single rubber sheet was 2.5-cm thick. According to research, stress is distributed in the N-S direction (Jiang et al., 2016) or the NW-SE direction (Yang, 2014). For the three hypothetical models described above, three series of six comparative experiments were designed (**Figure 11**):

1) Series I experiments. The first series of comparative experiments modeled the asymmetry of a basin structure with no pre-existing faults under two different stress directions (N-S direction and NW-SE direction). The sand thickness was 2.5 cm, and the deformation length was 6 cm. The baffles were pushed outward for 6 min at a speed of 0.5 cm/min, achieving a total stretching distance of 6 cm.
2) Series II experiments. The second series of comparative experiments modeled the asymmetry of a basin structure with NE-SW-striking pre-existing faults under two different stress directions (N-S direction and NW-SE direction). Plastic plates were used to simulate the pre-existing faults, inserted at a depth of 1.5 cm into the dry quartz sand and then covered with another 1 cm of dry quartz sand. The thickness of the sand was 4 cm above the double rubber sheet layer and 2.5 cm above the single rubber sheet layer, and the deformation length was 6 cm. The baffles were pushed outward for 6 min at a speed of 0.5 cm/min, achieving a total stretching distance of 6 cm.
3) Series III experiments. The third series of comparative experiments modeled the asymmetry of a basin structure with E-W-striking pre-existing faults under two different stress directions (N-S direction and NW-SE direction). Plastic plates were used to simulate the pre-existing faults, inserted at a depth of 1.5 cm into the dry quartz sand and then covered with another 1 cm of dry quartz sand. The thickness of the sand was 4 cm above the double rubber sheet layer and 2.5 cm above the single rubber sheet layer, and the deformation length was 6 cm. The baffles were pushed outward for 6 min at a speed of 0.5 cm/min, achieving a total stretching distance of 6 cm.

Modeling Results

Figures 12–14 show the results of the experiments as photographs taken at the top surface of the models (upper) with interpreted faults (lower), showing the fault populations at the end of the extension. All of the analyses used the target area of the models only to avoid lateral edge effects.

1) Series I: With no pre-existing faults under two different stress directions (N-S direction and NW-SE direction). The Series I experiments showed that a series of faults perpendicular to the direction of extensional stress were formed, which strike differently depending on the stress direction of the extension. Also, within these faults, no NE-SW-striking concealed faults were observed between E-W-striking faults (**Figure 12**). These results indicate that the formation and

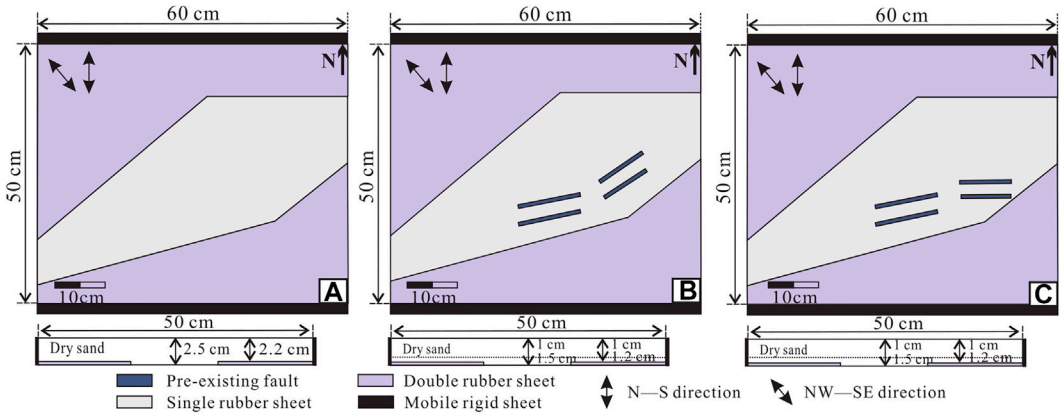

FIGURE 11 | Modeling of basin asymmetry. **(A)** Series I: With no pre-existing faults under two different stress directions (N-S direction and NW-SE direction). **(B)** Series II: With NE-SW-striking pre-existing faults under two different stress directions (N-S direction and NW-SE direction). **(C)** Series III: With E-W-striking pre-existing faults under two different stress directions (N-S direction and NW-SE direction).

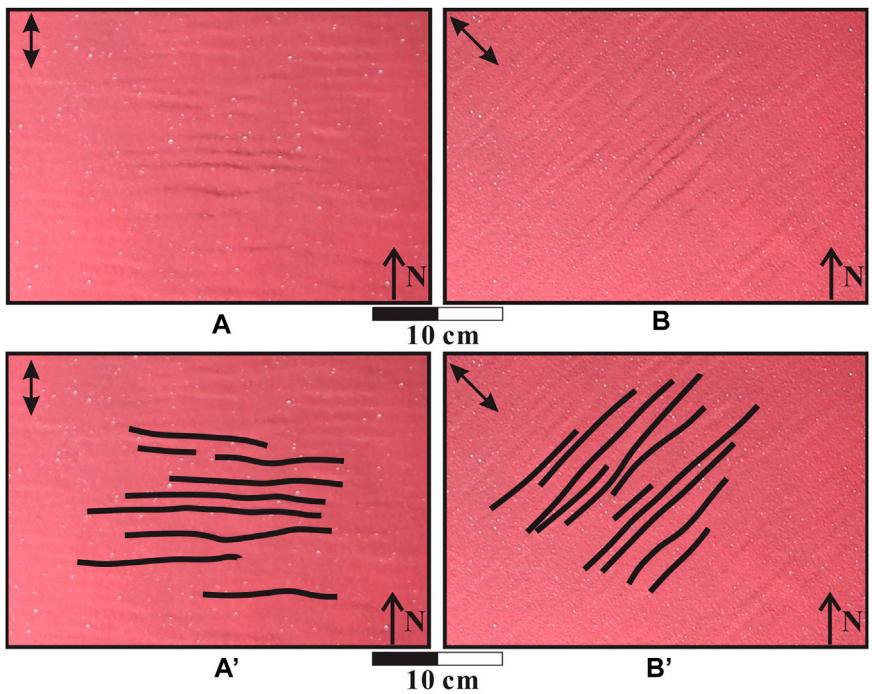

FIGURE 12 | Modeling results of Series I experiments. **(A)** A series of E-W-striking faults are formed under a N-S stress direction, indicated by the black lines in **(A')**. **(B)** A series of NE-SW-striking faults are formed under a NW-SE stress direction, indicated by the black lines in **(B')**.

strike of the new faults are not influenced by the asymmetry of the basin.

2) Series II: With NE-SW-striking pre-existing faults under two different stress directions (N-S direction and NW-SE direction). Under this scenario, the new faults formed with an arc extension appearing at the tail of the faults with increasing extension, and the E-W-striking fault developed at the transfer zone of the NE-SW-striking pre-existing faults under a N-S stress direction. In contrast, only small NE-SW-striking faults developed at the tail of the pre-existing faults, under a NW-SE stress direction (**Figure 13**). Whether under a NW-SE stress direction or N-S stress direction, E-W-striking main faults did not form when the pre-existing faults were NE-SW-striking. This is not consistent with observations in the Huawa area, and consequently, this hypothesis is not valid.
3) Series III: With E-W-striking pre-existing faults under two different stress directions (N-S direction and NW-SE

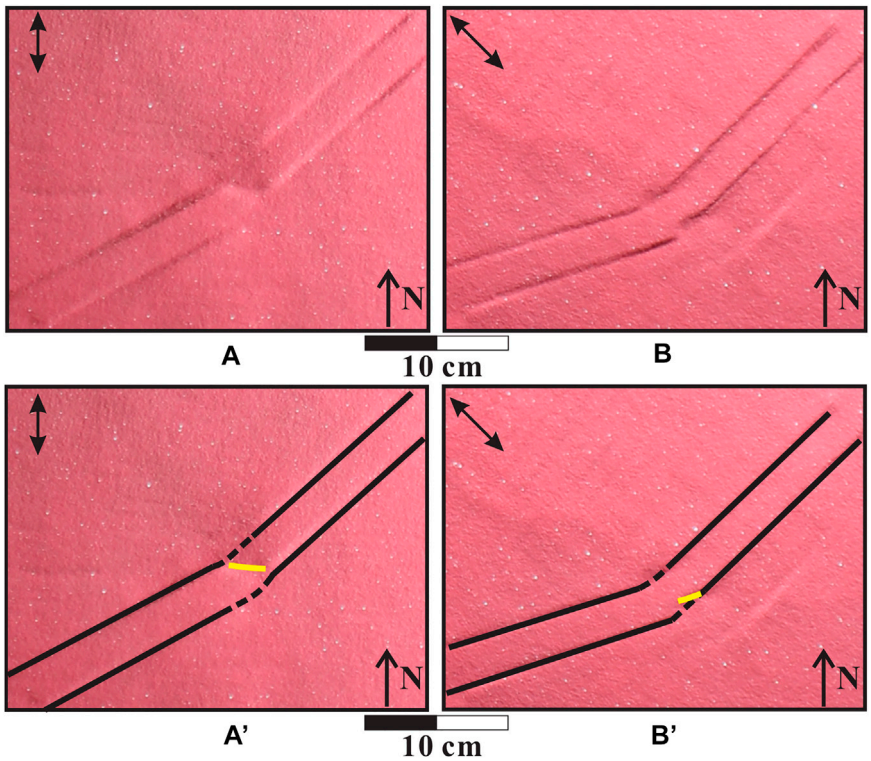

FIGURE 13 | Modeling results of Series II experiments. **(A)** An E-W-striking fault is formed at the transfer zone of the NE-SW-striking pre-existing faults under a N-S stress direction. **(B)** A small NE-SW-striking fault is formed at the tail of the NE-SW-striking pre-existing faults under a NW-SE stress direction. The faults are shown in **(A')** and **(B')**, where the black lines denote pre-existing faults, the black dotted lines denote the arc extension of pre-existing faults, and the yellow lines denote the new faults.

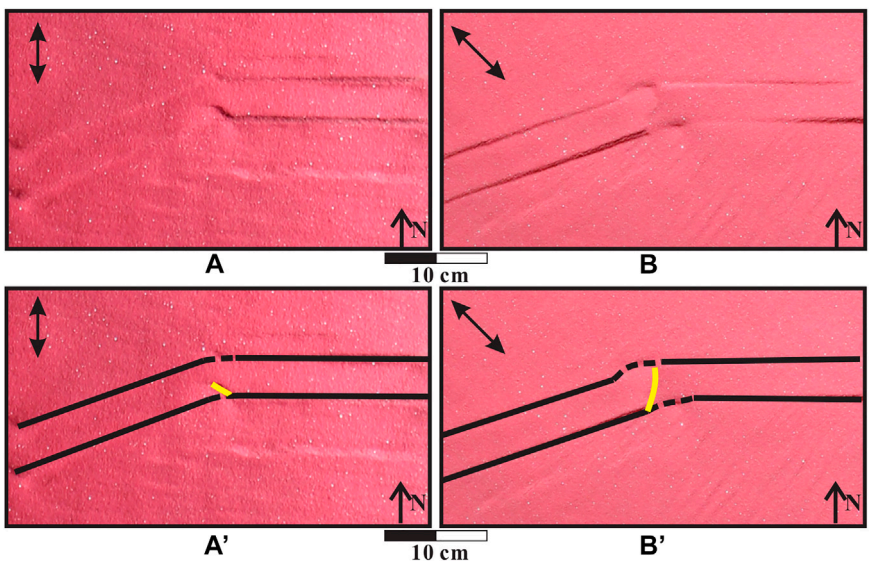

FIGURE 14 | Modeling results of Series III experiments. **(A)** A small NW-SE-striking fault is formed at the tail of the E-W-striking pre-existing faults under a N-S stress direction. **(B)** An NE-SW-striking fault is formed at the transfer zone of the E-W-striking pre-existing faults under a N-S stress direction. The faults are shown in **(A')** and **(B')**, where the black lines denote pre-existing faults, the black dotted lines denote the arc extension of pre-existing faults, and the yellow lines denote the new faults.

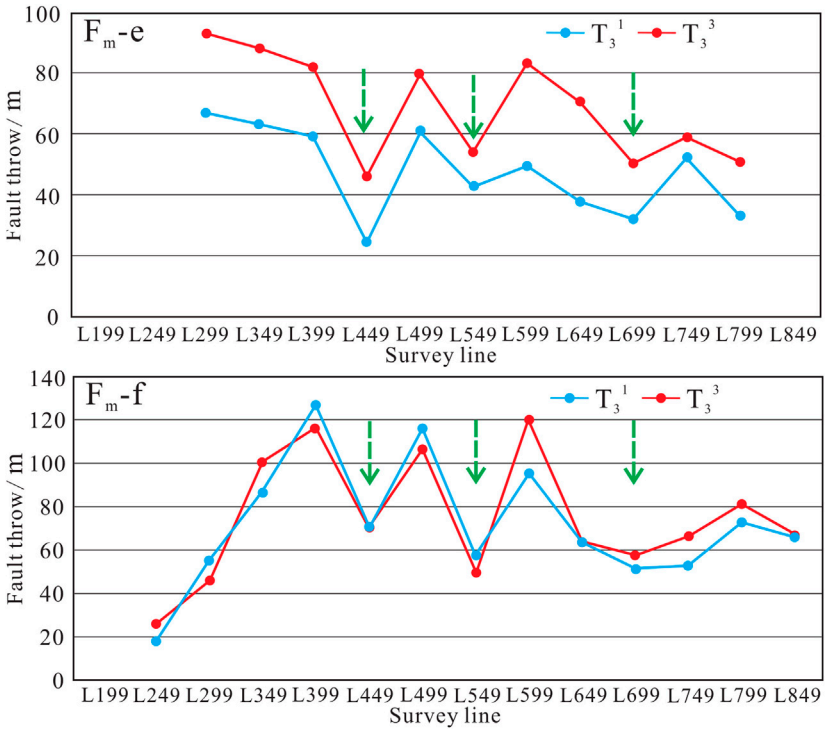

FIGURE 15 | Variation in the throw of E-W-striking main faults (F_m-e and F_m-f) at locations where NE-SW-striking concealed faults mechanically interact or link with E-W-striking main faults.

direction). Under this scenario, an arc extension appeared at the tail of the faults with increasing extension, and some NE-SW-striking faults developed between the transfer zone of the E-W-striking faults under a NW-SE stress direction. In contrast, only small NW-SE-striking faults developed at the tail of the E-W-striking pre-existing faults under a N-S stress direction (**Figure 14**). The results indicate that NE-SW-striking concealed faults develop at the transfer zone between E-W-striking pre-existing faults under a NW-SE stress direction. This is consistent with observations in the Huawa area, and this scenario most likely represents the formation mechanism of concealed faults in the Huawa area.

In conclusion, the experimental results show that the concealed faults in the Huawa area are formed in the transfer zone of pre-existing faults under the action of oblique extension stressing and have no relationship with the asymmetry of basin structure as they are not influenced by the asymmetry of the basin.

DISCUSSION

Based on the results of the experiments described previously, E-W-striking pre-existing faults under a NW-SE stress direction of extension are most likely the formation mechanism of concealed faults in the Huawa area. Under this scenario, the rift phase that follows will show reactivation in faults existing beforehand from the first rift stage and/or nucleation in second stage faults that developed recently in crust previously unruptured, which usually develop in a sub-perpendicular manner to the new extending direction (Cheng and Yang, 2003; Bailey et al., 2007; Gong et al., 2007; Henza et al., 2010; McHarg et al., 2019; Song and Cawood, 2015). Physical model simulations have been widely used to study how faults and fault interactions evolve (McClay and White, 1995; Chattopadhyay and Chakra, 2013). Moreover, the real 3D geometry of faults and fault interactions has been studied *via* an integrated 3D seismic reflection and borehole occurring in an artificial multi-phase fault network in the northern Horda Platform, northern North Sea (Duffy et al., 2015). On account of the above research, a broad range of fault interactions may occur within the first and second stage faults. The distribution of the throw on reactivated first stage faults can be adjusted when the faults have cross points or are impacted by faults of the second stage. This is consistent with observations in the Huawa area. In plan view, the throw does not vary smoothly along the strike of main faults; instead, the throw varies at locations where NE-SW-striking concealed faults mechanically interact or link with E-W-striking main faults (**Figure 15**). This phenomenon confirms the genesis mechanism of the NE-SW-striking concealed faults discussed in this paper and also suggests that we can predict the

development of concealed faults by the sudden change in the throw of the main faults.

During exploration activities conducted in the Huawa area of the Gaoyou Depression from 2004 to 2013, many concealed faults were found to control the formation of oil and gas traps, with the formation being more favorable at larger distances of concealed faults. This finding provides valuable knowledge for further development of oil and gas in this area.

SUMMARY AND CONCLUSIONS

In this paper, we present an integrated study that combines the use of 3D seismic and well-log datasets and laboratory experiments to study faults in the Huawa area of the Gaoyou sag, east China. The study reveals a network of NE-SW-striking concealed faults and E-W-striking main faults. The main findings are as follows:

1) Based on 3D seismic data mapping constrained by well-log data, we discovered that the NE-SW-striking concealed faults develop between E-W-striking main faults and that they are smaller than main faults in terms of extension length and fault throw.
2) The variation in the fault throw along with the growth index measured from the seismic data shows that concealed faults developed at the same time as or later than main faults.
3) Physical modeling conducted in the laboratory to simulate the development history of faults in our study area demonstrated that E-W-striking pre-existing faults under a NW-SE stress direction of extension are most likely the formation mechanism of concealed faults. Furthermore, variations in the throw of main faults occur at locations where NE-SW-striking concealed faults mechanically interact or link with each other, which is helpful for predicting the development of concealed faults.

DATA AVAILABILITY STATEMENT

The original contributions presented in the study are included in the article and in the Supplementary Material, further inquiries can be directed to the corresponding authors.

AUTHOR CONTRIBUTIONS

HH presented the idea and design of the research. HH and SH wrote the article and led the data analysis and interpreted the results with RZ, XF, CR, QL, WY, and YY. All authors contributed to the original article revision and approved it for publication.

FUNDING

This work was supported by the National Natural Science Foundation of China (No. 42002149) and the Natural Science Foundation of Heilongjiang Province (No. LH2021D007).

ACKNOWLEDGMENTS

The authors gratefully acknowledge the Science and Technology Innovation Team in Heilongjiang Province. The research topic of this team is “fault deformation, sealing, and fluid migration”.

REFERENCES

Bailey, C. M., Polvi, L. E., and Forte, A. M. (2007). “Pure Shear Dominated High-Strain Zones in Basement Terranes,” in *4-D Framework of Continental Crust: Geological Society of America Memoir* (Colorado, United States: Geological Society of America), 93–108. doi:10.1130/2007.1200(06)

Bellahsen, N., and Daniel, J. M. (2005). Fault Reactivation Control on normal Fault Growth: an Experimental Study. *J. Struct. Geol.* 27 (4), 769–780. doi:10.1016/j.jsg.2004.12.003.390

Byerlee, J., and Wyss, M. (1978). “Friction of Rocks,” in *Rock Friction and Earthquake Prediction* (Basel: Birkhauser), 615–626. doi:10.1007/978-3-0348-7182-2_4

Chattopadhyay, A., and Chakra, M. (2013). Influence of Pre-existing Pervasive Fabrics on Fault Patterns during Orthogonal and Oblique Rifting: An Experimental Approach. *Mar. Pet. Geol.* 39, 74–91. doi:10.1016/j.marpetgeo.2012.09.009

Chen, Q., Wu, L., and Zhou, Y. (2015). Hydrocarbon Accumulation Conditions and 400 Modes in the Area Around Shaobo Sub-sag, Gaoyou Sag. *J. China Univ. Mining Techn.* 44, 282–291. doi:10.13247/j.cnki.jcumt.000169

Cheng, S., and Yang, G. (2003). Fault Growth, Displacement Transfer and Evolution of the Jiugongkou Fault Overlap Zone on the Southern Marginal Fault Zone of the Guangling-Yuxian basin, north china. *Aust. J. Earth Sci.* 50 (1), 1–8. doi:10.1046/j.1440-0952.2003.00974.x

Deng, C., Gawthorpe, R. L., Finch, E., and Fossen, H. (2017). Influence of a Pre-existing Basement Weakness on normal Fault Growth during Oblique Extension: Insights from Discrete Element Modeling. *J. Struct. Geol.* 105, 44–61. doi:10.1016/j.jsg.2017.11.005

Dong, C., Zhen, L., Liu, Q., Luo, B., Li, C., and Wang, W. (2013). Accumulation System and Controlling Factors of Fault-Lithologic Reservoirs of Dainan Formation in Gaoyou Sag,northern Jiangsu basin. *Pet. Geology. Exp.* 35 (4), 395–400.

Duffy, O. B., Bell, R. E., Jackson, C. A.-L., Gawthorpe, R. L., and Whipp, P. S. (2015). Fault Growth and Interactions in a Multiphase Rift Fault Network: Horda Platform, Norwegian north Sea. *J. Struct. Geol.* 80, 99–119. doi:10.1016/j.jsg.2015.08.015

Gawthorpe, R. L., and Leeder, M. R. (2000). Tectono-sedimentary Evolution of Active Extensional Basins. *Basin Res.* 12, 195–218. doi:10.1046/j.1365-2117.2000.00121.x

Gong, L., Fu, X. F., Wang, Z. S., Gao, S., Jabbari, H., Yue, W. T., et al. (2019). A New Approach for Characterization and Prediction of Natural Fracture Occurrence in Tight-Oil Sandstones with Intense Anisotropy. *Am. Assoc. Pet. Geol. Bull.* 103 (6), 1383–1400. doi:10.1306/12131818054

Gong, L., Wang, J., Gao, S., Fu, X. F., Liu, B., Miao, F. B., et al. (2021). Characterization, Controlling Factors and Evolution of Fracture Effectiveness in Shale Oil Reservoirs. *J. Pet. Sci. Eng.* 203, 11. doi:10.1016/j.petrol.2021.108655

Handin, J. (1966). “Section 10: Strength and Ductility,” in *Handbook of Physical Constants* (Colorado, United States: Geological Society of America), 223–290. doi:10.1130/MEM97-p223

Henza, A. A., Withjack, M. O., and Schlische, R. W. (2010). Normal-fault Development during Two Phases of Non-coaxial Extension: An

Experimental Study. *J. Struct. Geol.* 32, 1656–1667. doi:10.1016/j.jsg.2009.07.007

Hu, X. (2010). On the Age and Origin of the Intrusive Rocks in Gaoyou Sag Ofnorth Jiangsu basin. *J. Stratigr.* 3, 293–297. doi:10.1017/S0004972710001772

Jiang, Q., Zhou, S., Zhu, G., Xie, C., Wang, Y., and Wu, J. (2016). Structural Characteristics and Prediction of the Concealed Faults in the Gaoyou Sag of Subei basin. *J. Geol.* 1, 250–254.

Krantz, D. E. (1991). A Chronology of Pliocene Sea-Level Fluctuations: The u.S. Middle atlantic Coastal plain Record. *Quat. Sci. Rev.* 10, 163–174. doi:10.1016/0277-3791(91)90016-n

Kulikowski, D., Amrouch, K., and Cooke, D. (2016). Geomechanical Modelling of Fault Reactivation in the Cooper Basin, Australia. *Aust. J. Earth Sci.* 63 (3), 295–314. doi:10.1080/08120099.2016.1212925

Li, Y. H. (2014). Trap Styles and Identification Technology of Concealed Faults in Gaoyou Sag. *J. China Univ. Pet.* 38 (04), 26–33. doi:10.3969/j.issn.1673-5005.2014.04.004

Liu, B., He, S., Meng, L., Fu, X., Gong, L., and Wang, H. (2021). Sealing Mechanisms in Volcanic Faulted Reservoirs in Xujiaweizi Extension, Northern Songliao Basin, Northeastern China. *Bulletin* 105, 1721–1743. doi:10.1306/03122119048

Liu, Y. X. (2017). The Study on the Evolution and Genetic Mechanism of Fault System in the Middle-Shallow Formations in Northern Daqing Placanticline. Master's thesis. Daqing: Northeast Petroleum University.

Maerten, L., Willemse, E. J. M., Pollard, D. D., and Rawnsley, K. (1999). Slip Distributions on Intersecting normal Faults. *J. Struct. Geol.* 21, 259–272. doi:10.1016/s0191-8141(98)00122-9

Mao, F. (2000). Determination of the Forming Time of Diabase in the Northern Slope of Gaoyou Sag and It's Relationship with Oil and Gas. *Pet. Explor. Develop.* 27, 2.

McClay, K. R., and White, M. J. (1995). Analogue Modelling of Orthogonal and Oblique Rifting. *Mar. Pet. Geol.* 12 (2), 137–151. doi:10.1016/0264-8172(95)92835-k

McHarg, S., Elders, C., and Cunneen, J. (2019). Normal Fault Linkage and Reactivation, Dampier sub-basin, Western australia. *Aust. J. Earth Sci.* 66 (2), 209–225. doi:10.1080/08120099.2019.1519848

Mei, L., Zhanghua, L., Aimin, J., Rong, Z., Changjian, S., Ying, Y., et al. (2013). Origin, Flow of Formation Water and Hydrocarbon Accumulation in the Zhenwu Area of the north Jiangsu basin, china. *Acta Geol. Sin.* 87, 819–829. doi:10.1111/1755-6724.12091

Ning, F., and Tang, L. (2009). Advances of Research on Physicalmodelling in Compressional Area. *Glob. Geol.* 28, 345–350. doi:10.13969/j.issn.1004-5589.2009.03.013

Qiu, X., Qian, S., Yu, W., and Liu, Q. (2016). Main Achievements, New Understanding and Technological Progress for Oil and Gas Exploration in north Jiangsu basin during the 12~(th) Five-Year Plan. *China Pet. Explor.* 21, 62.

Rashidi, A. (2021). Geometric and Kinematic Characteristics of the Khazar and north Alborz Faults: Links to the Structural Evolution of the north Alborz-South Caspian Boundary, Northern iran. *J. Asian Earth Sci.* 213, 104755. doi:10.1016/j.jseaes.2021.104755

Rotevatn, A., and Fossen, H. (2011). Simulating the Effect of Subseismic Fault Tails and Process Zones in a Siliciclastic Reservoir Analogue: Implications for Aquifer Support and Trap Definition. *Mar. Pet. Geol.* 28 (9), 1648–1662. doi:10.1016/j.marpetgeo.2011.07.005

Ryan, L., Magee, C., and Jackson, A. L. (2017). The Kinematics of normal Faults in the Ceduna Subbasin, Offshore Southern Australia: Implications for Hydrocarbon Trapping in a Frontier basin. *Aapg Bull.* 101 (3), 321–341. doi:10.1306/08051615234

Schellart, W. P. (2000). Shear Test Results for Cohesion and Friction Coefficients for Different Granular Materials: Scaling Implications for Their Usage in Analogue Modelling. *Tectonophysics* 324, 1–16. doi:10.1016/S0040-1951(00)00111-6

Song, T., and Cawood, P. A. (1999). Multistage Deformation of Linked Fault Systems in Extensional Regions: an Example from the Northern Perth basin, Western australia. *Aust. J. Earth Sci.* 46 (6), 897–903. doi:10.1046/j.1440-0952.1999.00752.x

Sun, Y., and Lu, L. (2017). Structural Evolution of Thrust-Related Folds and Associated Fault Systems in the Eastern Portion of the Deep-Water Niger Delta. *Mar. Pet. Geol.* 92, 234–254. doi:10.1016/j.marpetgeo.2017.12.012

Thorsen, C. E. (1963). Age of Growth Faulting in Southeast Louisiana. *Trans. Gulf Coast Assoc. Geol. Societies* 13, 103–110.

Uchida, H., Mukoyoshi, H., Tonai, S., Yamaguchi, M., and Kobayashi, K. (2021). Reactivation of Minor Faults in a Blind Active Fault Area: a Case Study of the Aftershock Area of the 2000 Western Tottori Earthquake, japan. *J. Asian Earth Sci. X* 5, 100053. doi:10.1016/j.jaesx.2021.100053

Wang, B. R., Qi, D., Wang, E., Wei, S., and Liang, X. (2001). Characteristics of the Diabase and Altered Zone in Bxp Area of Subei basin and Relationship 480 between the Diabase and the Formation of Hydrocarbon Reservoir. *J. Xi'an Pet. Inst. (Natural Science)* 6, 5–7+5.

Wang, H. Y., Fu, X. F., Wang, H. X., Chen, M., Meng, L. D., and Ping, G. D. (2020). Study on the Control of Quantitative Analysis and Evaluation of Fault Activity on Hydrocarbon Accumulation in Qikou Sag, Bohai Bay Basin. *Acta Geol. Sin.* 94 (10), 3062–3073. doi:10.19762/j.cnki.dizhixuebao.2020274

Wang, Q. (2018). The Deformation Mechanism of the Tectonic and the Study of its Sand-Box Analog Models in Xujiaweizi Fault Depression. Master's Thesis. Daqing: Northeast Petroleum University.

Whipp, P. S., Jackson, C. A.-L., Gawthorpe, R. L., Dreyer, T., and Quinn, D. (2014). Normal Fault Array Evolution above a Reactivated Rift Fabric; a Subsurface Example from the Northern Horda Platform, Norwegian north Sea. *Basin Res.* 26 (4), 523–549. doi:10.1111/bre.12050

Yang, L. (2014). The Structural Evolution in the Cenozoic of Subei basin and its Relationship with Oil and Gas. Master's Thesis. Hubei, China: School of Geosciences Yangtze University.

Yang, Q., and Chen, H. (1989). Ectonic Evolution of the north Jiangsu-South Yellow 490 Sea basin. *Pet. Geol. Exp.* 25, 250–254. doi:10.11781/sysydz198903250

Zhao, M. (1989). Discussion on the Growth index of Fault. *Pet. Geol. Exp.* 11, 250–254. doi:10.11781/sysydz198903250

Zhao, S., Zhao, X., and Yang, S. (2005). Similar Analysis of Geological Structure Physical Model. *Northwest. Geol.* 38, 14–18. doi:10.1016/j.measurement.2005.02.005

Conflict of Interest: The authors declare that the research was conducted in the absence of any commercial or financial relationships that could be construed as a potential conflict of interest.

Publisher's Note: All claims expressed in this article are solely those of the authors and do not necessarily represent those of their affiliated organizations, or those of the publisher, the editors and the reviewers. Any product that may be evaluated in this article, orclaim that may be made by its manufacturer, is not guaranteed or endorsed by the publisher.